

Polarization of chirality

David Ayuso^{1*}, Andres Ordonez^{1,2*}, Piero Decleva³, Misha Ivanov^{1,4,5}, Olga Smirnova^{1,2}

¹*Max-Born-Institut, Berlin, Germany*

²*Technische Universität Berlin, Berlin, Germany*

³*Dipartimento di Scienze Chimiche e Farmaceutiche, Università degli Studi di Trieste, Trieste, Italy*

⁴*Institute für Physik, Humboldt-Universität zu Berlin, Berlin, Germany*

⁵*Department of Physics, Imperial College London, London, UK*

**These authors contributed equally to this work*

It has been long recognized that the spatial polarization of the electronic clouds in molecules, and the spatial arrangements of atoms into chiral molecular structures, play crucial roles in physics, chemistry and biology. However, these two fundamental concepts – chirality ^{1,2} and polarization³ – have remained unrelated so far. This work connects them by introducing and exploring the concept of polarization of chirality. We show that, like charge, chirality, or handedness, can be polarized, and that such polarization leads to fundamental consequences, demonstrated here using light. First, we analyze how chirality dipoles and higher-order chirality multipoles manifest in experimental observables. Next, we show how to create chirality-polarized optical fields of alternating handedness in space. Despite being achiral, these racemic space-time light structures interact differently with chiral matter of opposite handedness, and the chirality dipole of light controls and quantifies the strength

of the enantio-sensitive response. Using nonlinear interactions, we can make a medium of randomly oriented chiral molecules emit light to the left, or to the right, depending on the molecular handedness and on the chirality dipole of light. The chiral dichroism in emission direction reaches its highest possible value of 200%. Our work opens the field of chirality polarization shaping of light and new opportunities for efficient chiral discrimination and control of chiral and chirality-polarized light and matter on ultrafast time scales.

Chirality, or handedness, is a ubiquitous property of light and matter characterized by an unusual type of symmetry – mirror symmetry. Mirror reflection transforms a chiral object into its opposite counterpart, with our left and right hands being a typical example. These mirror twins are called enantiomers, and symmetry dictates that they must behave identically unless interacting with another chiral object. Handedness changes sign upon reflection: two enantiomers are characterized by the handedness of opposite sign. In this sense, handedness is similar to charge: just like a collection of charges can be positive, negative or neutral, a collection of chiral objects can have positive, negative, or zero total handedness (the latter called racemic mixtures). Chirality is of tremendous importance in nature and distinguishing molecular enantiomers is vital, which has stimulated a major recent research effort^{4–20}. Just as important is the role of spatial polarization of electronic clouds in molecules, from controlling how fatty acids dissolve in water to giving specificity to the biological activity of enzymes²¹. Polarization of charge characterizes overall neutral but non-uniform spatial charge distributions and their interaction with other charges. Following our parallel between distribution of charge and distribution of handedness (see Fig. 1), one would expect *polarization of chirality* to play an important role in the interaction between extended chiral

objects displaying a position dependent chirality. Is this expectation correct? Can we engineer such structures? How effective is their interaction with chiral media and how can it be characterized? Can polarization of chirality be detected in an experiment? Here we give positive answers to these fundamental questions.

Let us begin with the simple case depicted in Fig. 1a: a one-dimensional arrangement of alternating positive and negative charges $\pm q$. When the particles are uniformly distributed, the medium is not polarized. It becomes polarized as we modify their positions, creating dipoles $\mathbf{d}_e = q\mathbf{r}_0$, where \mathbf{r}_0 is the vector connecting the nearby negative and positive charges. Consider now a similar racemic distribution of chiral units of alternating handedness, Fig. 1b. These units can be chiral particles or chiral light fields. Just like the neutral medium of charged particles, this racemic distribution is unpolarized if the distances between consecutive chiral units are the same. If we modify them, e.g. by shifting the right-handed units to the left, we create *dipoles of chirality*, and the medium acquires *polarization of chirality*. We could define the dipole of chirality as $\mathbf{d}_c = h\mathbf{r}_0$, where \mathbf{r}_0 is the vector connecting the nearby left and right-handed units and $h = h_R = -h_L$ is the handedness of a single unit.

However, the definition of the unit cell in Fig. 1a, together with the polarization of the unit cell, is not unique, a well-known problem encountered in solid state physics²². Therefore, the concept of *chirality dipole* should rely on specific observables. In this context, consider the interaction of chiral matter with chiral light. Traditionally, chiro-optical effects have relied on the interaction with both the electric and magnetic field components of a circularly polarized light

wave. However, the magnetic interaction occurs beyond the electric-dipole approximation and is often very weak. This limitation can be bypassed in a particularly straightforward manner by using a pair of non-collinear laser beams. These allow us to engineer propagating optical fields with three orthogonal polarization components^{23–26} and create synthetic chiral light²⁵. Such light is chiral already in the electric-dipole approximation: the electric field of light draws a chiral Lissajous figure in every point in space²⁵. The chiro-optical response to this light does not rely on magnetic interactions and is orders of magnitude stronger. While synthetic chiral light is chiral in every point in space, its handedness can be distributed in space as desired. Thus, it is ideally suited to model distributed handedness and test the concept of *polarization of chirality*.

The enantio-sensitive optical response to chiral light originates from the interference of two contributions to the light-induced polarization $\mathbf{P}_\omega = \mathbf{P}_\omega^{ACH} + \mathbf{P}_\omega^{CH}$ at a given frequency ω , one of them not sensitive to chirality (\mathbf{P}_ω^{ACH}), and the other unique to chiral matter (\mathbf{P}_ω^{CH}), which is out of phase in media of opposite handedness. The microscopic intensity $|\mathbf{P}_\omega|^2$ is sensitive to the interference of $\mathbf{P}_\omega^{CH}(\mathbf{r})$ and $\mathbf{P}_\omega^{ACH}(\mathbf{r})$ at the same point \mathbf{r} through the term $\mathbf{P}_\omega^{ACH*}(\mathbf{r}) \cdot \mathbf{P}_\omega^{CH}(\mathbf{r}) + \text{c.c.}$ This interference encodes the distributed handedness of light or matter (or both). That is, the near-field response records the distributed handedness locally. In contrast, the far-field signal provides access to the interference of the chiral and achiral contributions from the whole interaction region and is sensitive to spatial correlations of $\mathbf{P}_\omega^{ACH}(\mathbf{r})$ and $\mathbf{P}_\omega^{CH}(\mathbf{r} + \mathbf{r}')$. The far-field signal maps the distribution of handedness on observables such as the enantio-sensitive direction of light emission and the enantio-sensitive shape of the emission pattern on the screen. These observables are simply the different moments of the enantio-sensitive component of the intensity distribution

in the reciprocal space, which is proportional to the real part of

$$\tilde{G}_\omega(\mathbf{k}) = \tilde{\mathbf{P}}_\omega^{ACH*}(\mathbf{k}) \cdot \tilde{\mathbf{P}}_\omega^{CH}(\mathbf{k}). \quad (1)$$

(The subscript ω indicates that we consider far-field signal centered at frequency ω with bandwidth $\Delta\omega \ll \omega$, hence $\Delta k \ll k$; we omit this subscript below for brevity.) For example, the enantio-sensitive contribution to the total intensity and the average direction of emission are given by the zero and first moments of the distribution, respectively:

$$\langle \Delta I_\omega \rangle \propto \int d^3k \tilde{G}(\mathbf{k}) + \text{c.c.}, \quad \langle k_i \rangle = \int d^3k k_i \tilde{G}(\mathbf{k}) + \text{c.c.} \quad (2)$$

The enantio-sensitive shape of the emission pattern on the screen is given by the higher moments:

$$\langle k_{i,j,\dots} \rangle = \int d^3k k_i k_j \dots \tilde{G}(\mathbf{k}) + \text{c.c.}, \quad (3)$$

Eqs. (2-3) describe the multipoles of the enantio-sensitive intensity distribution in k -space. The different moments of $\tilde{G}(\mathbf{k})$ reflect the fact that handedness can have complex distributions both in coordinate and reciprocal space.

If the handedness of matter is distributed uniformly, then $\tilde{G}(\mathbf{k})$ reflects the distributed handedness of light $\tilde{h}(\mathbf{k})$, $\tilde{G}(\mathbf{k}) \propto \tilde{h}(\mathbf{k})$. The enantio-sensitive contribution to light intensity, the direction of light emission, the shape of the light spot on a screen will then encode zero, first, and higher order moments of $\tilde{h}(\mathbf{k})$:

$$h_0 = \int d^3k \tilde{h}(\mathbf{k}), \quad \tilde{\mathbf{h}} = \int d^3k \mathbf{k} \tilde{h}(\mathbf{k}), \quad \tilde{h}_{\{ij,\dots\}} = \int d^3k k_i k_j \dots \tilde{h}(\mathbf{k}). \quad (4)$$

The enantio-sensitive contribution to the total intensity is only non-zero if light's handedness is non-zero on average, $h_0 \neq 0$. But even if $h_0 = 0$, enantio-sensitive effects remain. For example,

if light is racemic, $h_0 = 0$, but chirality polarized, i.e. $\tilde{\mathbf{h}} \neq 0$, we will see enantio-sensitive deflection in the nonlinear optical response. In general, the distributed handedness of racemic objects manifests itself in an entire array of tensorial enantio-sensitive observables. Their measurement requires acquisition of N -dimensional data sets, where N is the rank of the corresponding tensor.

We now illustrate this general analysis with a specific example and demonstrate that racemic, chirality-polarized light can be used to discriminate chiral molecules with extremely high efficiency. Chirality-polarized light can be created using two beams propagating in the xy plane, at small angles $\alpha = \pm 5^\circ$ with respect to the y axis, as shown in Fig. 2a. Both contain a fundamental field, linearly polarized in the plane of propagation, and a weak second harmonic component polarized orthogonal to this plane. In the overlap region, the total electric field is elliptically polarized in the xy plane at frequency ω , and it has a weak, linearly polarized, 2ω frequency component along z ,

$$\mathbf{F}(x, t) = \Re \left\{ [F_x(x)\hat{\mathbf{x}} + iF_y(x)\hat{\mathbf{y}}]e^{-i\omega t} + F_z(x)e^{-2i(\omega t + \phi)}\hat{\mathbf{z}} \right\} \quad (5)$$

where the two-color phase delay $\phi = \frac{\phi_1 + \phi_2}{2}$, which controls the field's handedness, is determined by the two-colour phase delays in the individual beams, ϕ_1 and ϕ_2 . The spatial modulation of the three orthogonal polarization components, F_x , F_y and F_z , is presented in Fig. 2b. The electric field vector, at a given point in space, draws a chiral Lissajous figure in \mathbf{F} -space. Fig. 2c shows that field's transverse spin $\mathbf{S}_{2\omega} \propto \mathbf{F}_\omega^* \times \mathbf{F}_\omega \propto F_x F_y \hat{\mathbf{z}}$ and $\mathbf{F}_{2\omega} = F_z \hat{\mathbf{z}}$ change sign at different positions. As a result, the sign of their product $\mathbf{S}_{2\omega} \cdot \mathbf{F}_{2\omega}$, which determines the sign of light's handedness, changes periodically in space. This spatial distribution of field's handedness in the near field is recorded in the non-linear response of the medium. In the lowest order of non-linearity, the

strength of the local enantio-sensitive response is controlled by the chiral correlation function²⁵ $h^{(5)} \propto \mathbf{S}_{2\omega} \cdot \mathbf{F}_{2\omega} |\mathbf{F}_\omega|^2$ shown in Fig. 2d. We see a periodic structure of “dimers” of alternating handedness, the structure envisioned in Fig. 1b. The overall light field has mirror symmetry with respect to the yz plane (up to a global time shift) and is achiral. However, its handedness is polarized, with the x -component of the dipole of chirality (Eq. 4) equal to:

$$\tilde{h}_x \propto \cos(\phi_2 - \phi_1) e^{i(\phi_1 + \phi_2)} \quad (6)$$

where ϕ_1 and ϕ_2 are the two-colour phase delays in each of the two beams (see Fig. 2). The difference $\phi_2 - \phi_1$ controls the amplitude of $\tilde{\mathbf{h}}$, which maximizes for $\phi_1 = \phi_2$. The phase of $\tilde{\mathbf{h}}$ is controlled by $\phi_1 + \phi_2$. This gives us control over the polarization of the field’s handedness: we set $\phi_1 = \phi_2$ to maximize its strength, and then vary ϕ_1, ϕ_2 synchronously to control the orientation of $\tilde{\mathbf{h}}$ in the complex plane. Note that the polarization of the field handedness in position space, evident in Fig. 2d, leads to a non-zero value of $\int h^{(5)} x dx$, which is proportional to \tilde{h}_x for this definition of the unit cell.

We now analyze the interaction of the chirality-polarized light field depicted in Fig. 2 with chiral matter. Fig. 3 shows the nonlinear response of left- and right-handed randomly oriented fenchone molecules driven by the field in Fig. 2. The fundamental wavelength of the incident field is 1300 nm with intensity $7.5 \cdot 10^{12} \text{ W}\cdot\text{cm}^{-2}$ in each beam; the second harmonic intensity is 100 times weaker, and we calculate the response polarized along z . Panels a,b show the intensity and phase of harmonic 12 (for other harmonics, see Supplementary Information). The response of opposite molecular enantiomers is antisymmetric with respect to x ; the effect of exchanging the molecular enantiomer is equivalent to reversing the polarization of chirality of the field, which can

be done by shifting the two-colour phase delay in both beams (see Eq. 6).

The single-molecule response, at a given point space, is enantio-sensitive in intensity (Fig. 3a) because the driving field is locally chiral. However, the overall light field is achiral, and thus the total intensity signal, obtained after integration over x , is identical in left- and right-handed molecules. Still, the direction of polarization of the field’s handedness is imprinted in the phase of the nonlinear response, which depends strongly on the molecular handedness (Fig. 3b): the slope of the phase dependence on x is positive for right-handed molecules and negative in left-handed molecules. These enantio-sensitive phase gratings control the direction of macroscopic harmonic emission in the far field. The strength of this effect is controlled by the dipole of chirality \tilde{h}_x , which determines the deflection angle.

Fig. 4a shows the harmonic 12 intensity in the far field. The total (angle-integrated) intensity is the same for left- and right-handed molecules, as in the near field (Fig. 3a). However, the direction of emission is extremely enantio-sensitive: while the left-handed molecules emit harmonics to the left (towards negative x), the right-handed molecules emit harmonics to the right (positive x). We control the enantio-sensitive direction of emission by controlling the polarization of the field’s handedness in our setup (see Eq. 6). Fig. 4b shows that chiral dichroism resolved in the emission angle reaches the ultimate efficiency limit, $CD = 200\%$ (Fig. 4b). We find giant enantio-sensitivity in the direction of emission of all even harmonics, see Supplementary Information.

We can define the left-right asymmetry in the harmonic emission as $A_{LR} = 2\frac{I_L - I_R}{I_L + I_R}$, where I_L and I_R are the intensities of harmonic emission to the left ($\beta < 0$) and to the right ($\beta > 0$),

respectively. This angle-integrated quantity reaches very high values for all harmonic numbers, as shown in Fig. 4c. The direction of harmonic emission is correlated to the enantiomeric excess of the medium $ee = \frac{C_R - C_S}{C_R + C_S}$, with C_R and C_S being the concentrations of the right- and left-handed molecules, see Fig. 4d. The expectation value of the emission angle is then given by

$$\langle \beta \rangle = \frac{ee \tilde{I}_{aR}}{\tilde{I}_a^\beta + ee^2 \tilde{I}_R^\beta} \quad (7)$$

where \tilde{I}_{aR} , \tilde{I}_a^β and \tilde{I}_R^β are angle-integrated quantities that do not depend on ee . Eq. 7 allows us to quantify small values of enantiomeric excess in macroscopic mixtures.

Polarization of chirality is a powerful concept which allows one to engineer highly efficient chiral interactions of racemic objects. It opens several opportunities. The first stems from flexibility in chiral polarization shaping of synthetic chiral light, where the spatial dependence of the field's transverse spin $\mathbf{S}_{\omega_n}^{(n)}(\mathbf{r})$ and the electric field component $\mathbf{F}_{\omega_n}(\mathbf{r})$ parallel to it can be controlled separately. Here one can take full advantage of modern light shaping techniques including polarization shaping in space and time²⁷⁻²⁹. In contrast, in standard circularly polarized light, this opportunity is limited, since its electric and magnetic components are locked to each other. A non-zero dipole of chirality is present in any locally chiral field^{25,26} where field's transverse spin $\mathbf{S}_{\omega_n}^{(n)}(\mathbf{r})$ and $\mathbf{F}_{\omega_n}(\mathbf{r})$ have opposite parity.

The second opportunity is to use chirality polarized light to imprint polarization of chirality onto racemic matter, creating "chiral polaritons". The phase relationship between the imparted angular momentum and polarization waves, induced in the medium by chirality-polarized light, will define the medium chiral polarization, its coherence length, and the strength of its interaction

with other chiral structures.

The third opportunity is to exploit giant enantio-sensitivity to not only create chirality-polarized matter, but also to control it on ultrafast time scales. Chirality-polarized light may allow us to identify racemic aggregates of chiral matter that exhibit complex chirality patterns in space, and to quantify their degree of polarization of chirality.

Finally, polarization of chirality can also be used for efficient separation of opposite enantiomers in racemic mixtures by extending the proposal of Ref.³⁰ to chirality polarized light, which would allow one to bypass the use mechanical transition gratings and weak magnetic field interactions.

Acknowledgements

DA, AO, MI and OS acknowledge support from the DFG SPP 1840 “Quantum Dynamics in Tailored Intense Fields” and DFG grant SM 292/5-1. MI acknowledges MURI grant EP/N018680/1.

Competing Interests

The authors declare that they have no competing financial interests. The data that support the plots within this paper and other findings of this study are available from the corresponding authors upon reasonable request. Correspondence should be addressed to david.ayuso@mbi-berlin.de, andres.ordonez@mbi-berlin.de and olga.smirnova@mbi-berlin.de.

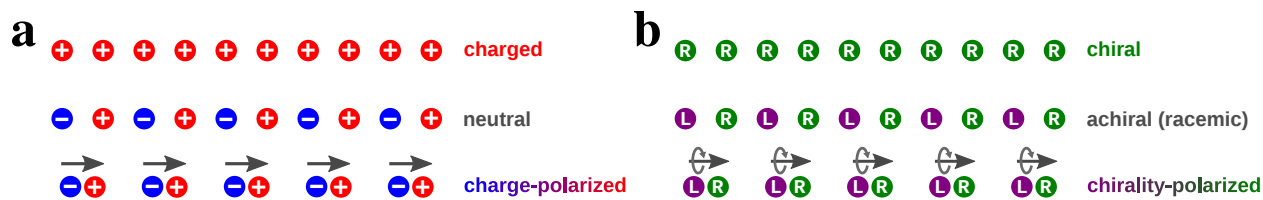


Figure 1: **Polarization of charge versus polarization of chirality.** **a**, Mono-dimensional (1D) arrangement of charged units that is: charged and unpolarized, neutral and unpolarized, and neutral and polarized. **b**, 1D arrangement of chiral units that is: chiral and unpolarized, achiral and unpolarized, and achiral and polarized.

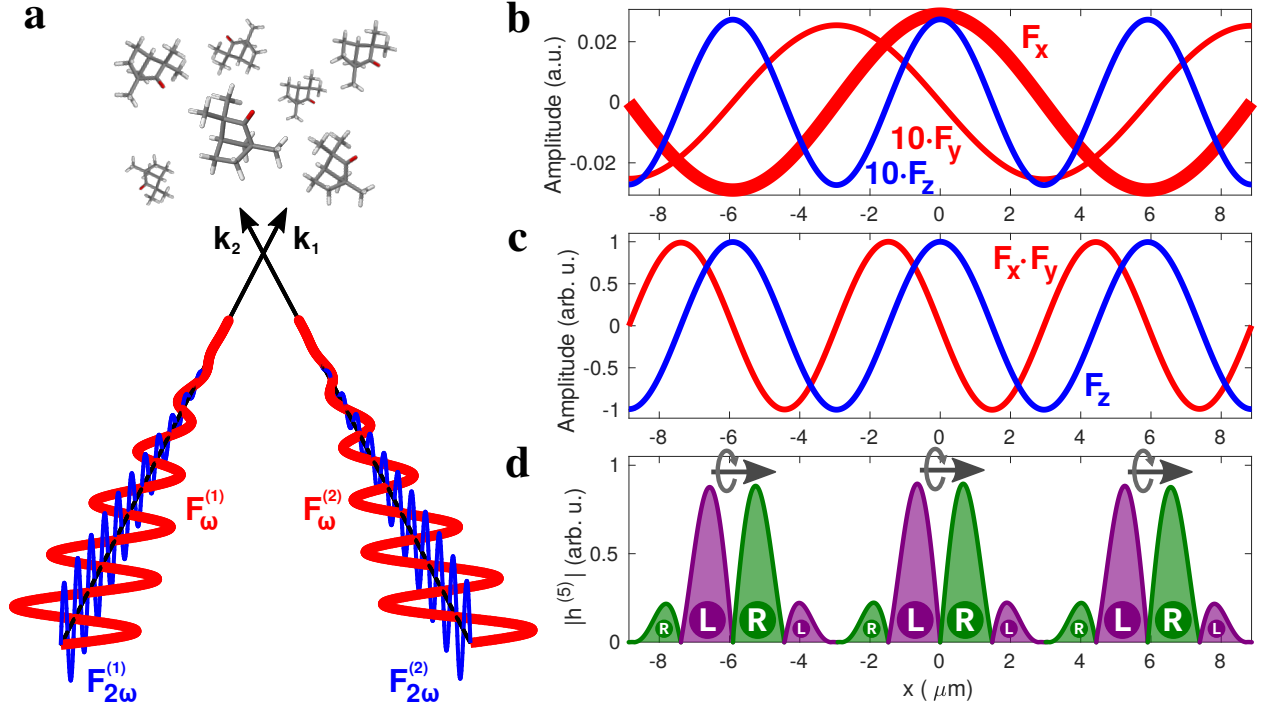


Figure 2: **Racemic space-time “crystal” with polarization of handedness.** **a**, Setup for creating chirality polarized light. Two non-collinear beams carry an ω field, linearly polarized in the xy propagation plane, and an orthogonally polarized 2ω field, with the same two-color delay in both beams. **b**, Amplitudes of the x , y and z field components in the overlap region, for $\omega = 0.044\text{a.u.}$ ($\lambda = 1030\text{nm}$), $F_{\omega}^{(1)} = F_{\omega}^{(2)} = 0.0146\text{a.u.}$, $F_{2\omega}^{(1)}/F_{\omega}^{(1)} = F_{2\omega}^{(2)}/F_{\omega}^{(2)} = \sin(\alpha)$; $2\alpha = 10^\circ$ is the angle between the beams, the focal diameter is 200nm . **c**, Normalized 2ω -field amplitude (F_z) and transverse spin $\propto F_x F_y$. **d**, Local handedness of the light field, characterized by its fifth-order chiral correlation function $h^{(5)}$. The colours encode the phase of $h^{(5)}$ and thus the field’s handedness, which is controlled by the relative phase ϕ (see Eq. 5); purple: $\arg\{h^{(5)}\} = 2\phi + 0.5\pi$, green: $\arg\{h^{(5)}\} = 2\phi - 0.5\pi$. The grey arrows indicate the direction of polarization of chirality.

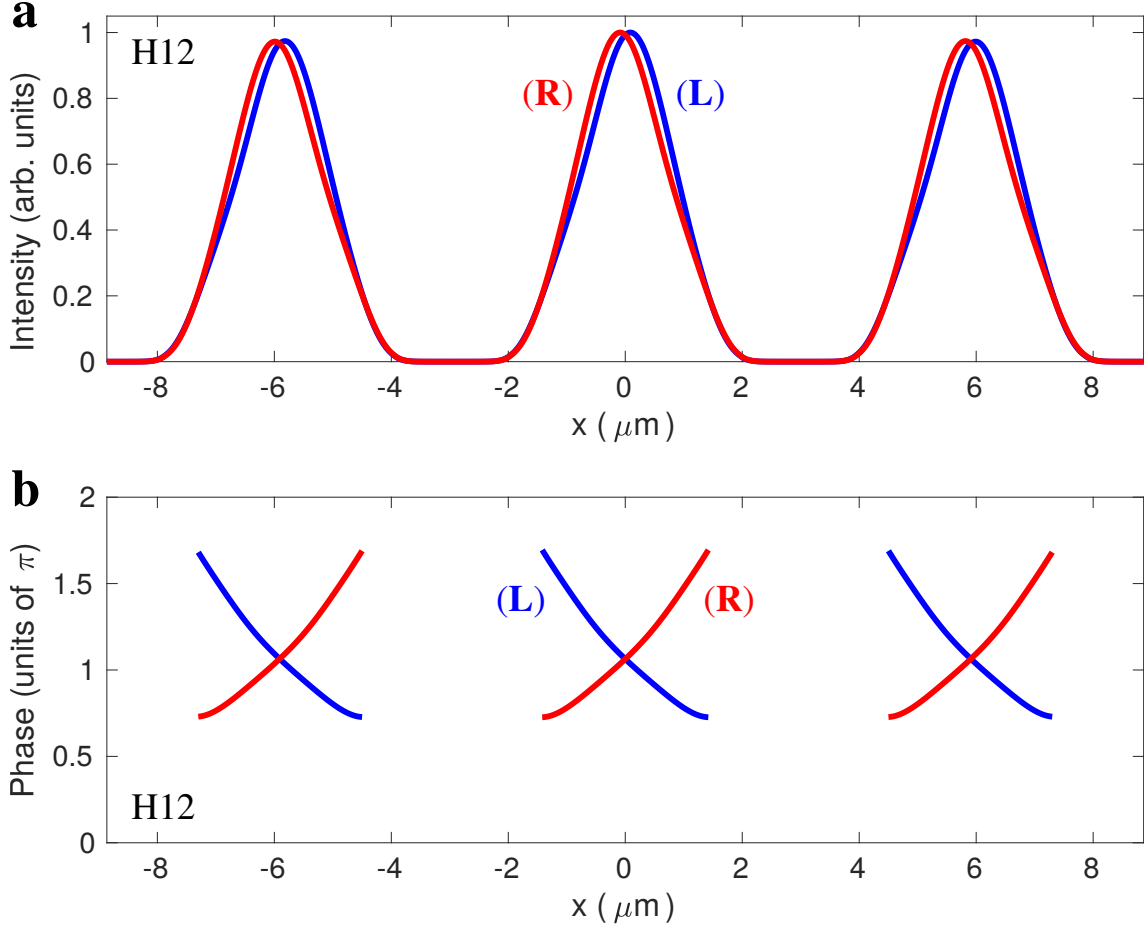


Figure 3: **Enantio-sensitive non-linear response of chiral matter to chirality-polarized light.**

Intensity (a) and phase (b) of the nonlinear response driven by the space-time light structure presented in Fig. 2 in randomly oriented left-handed (blue) and right-handed (orange) fenchone molecules at frequency 12ω ; $\lambda = 1030\text{nm}$, $F_{\omega}^{(1)} = F_{\omega}^{(2)} = 0.0146\text{a.u.}$, $F_{2\omega}^{(1)}/F_{\omega}^{(1)} = F_{2\omega}^{(2)}/F_{\omega}^{(2)} = 0.1$, $\alpha = 5^\circ$, the focal diameter 200nm .

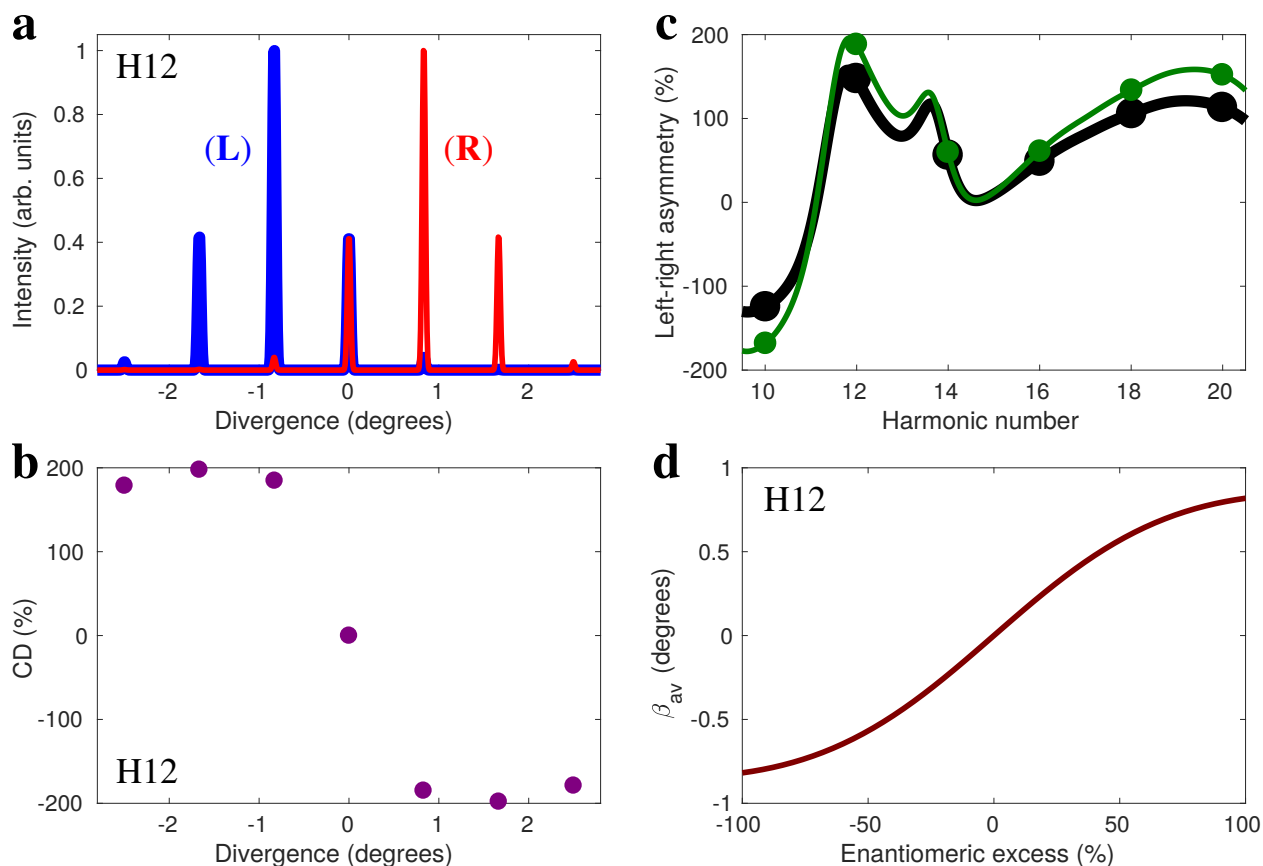


Figure 4: **Macroscopic high harmonic generation.** **a**, Macroscopic high harmonic emission at frequency 12ω from left-handed (blue) and right-handed (red) randomly oriented fenchone molecules as a function of the emission angle. Field parameters are the same as in Fig.3. **b**, Chiral dichroism, $CD = 2 \frac{I_L - I_R}{I_L + I_R}$. **c**, Left-right asymmetry in the macroscopic emission of even harmonics from 10 to 20, calculated including (black) or not including (green) the central emission peak. **d**, Mean value of the emission angle as a function of the enantiomeric excess.

1. Blaser, H.-U. Chirality and its implications for the pharmaceutical industry. *Rendiconti Lincei* **24**, 213–216 (2013). URL <https://doi.org/10.1007/s12210-012-0220-2>.

2. Berova, N., Polavarapu, P. L., Nakanishi, K. & Woody, R. W. *Comprehensive Chiroptical Spectroscopy* (Wiley, 2013).
3. Slater, J. & Frank, N. *Electromagnetism*. Dover Books on Physics (Dover Publications, 2012).
URL <https://books.google.de/books?id=hsDDAgAAQBAJ>.
4. Nahon, L., Garcia, G. A. & Powis, I. Valence shell one-photon photoelectron circular dichroism in chiral systems. *Journal of Electron Spectroscopy and Related Phenomena* **204**, 322–334 (2015). URL <http://www.sciencedirect.com/science/article/pii/S0368204815000766>. Gas phase spectroscopic and dynamical studies at Free-Electron Lasers and other short wavelength sources.
5. Ritchie, B. Theory of the angular distribution of photoelectrons ejected from optically active molecules and molecular negative ions. *Phys. Rev. A* **13**, 1411–1415 (1976). URL <https://link.aps.org/doi/10.1103/PhysRevA.13.1411>.
6. Powis, I. Photoelectron circular dichroism of the randomly oriented chiral molecules glyceraldehyde and lactic acid. *The Journal of Chemical Physics* **112**, 301–310 (2000). URL <https://doi.org/10.1063/1.480581>.
7. Böwering, N. *et al.* Asymmetry in photoelectron emission from chiral molecules induced by circularly polarized light. *Phys. Rev. Lett.* **86**, 1187–1190 (2001). URL <https://link.aps.org/doi/10.1103/PhysRevLett.86.1187>.

8. Fischer, P. & Hache, F. Nonlinear optical spectroscopy of chiral molecules. *Chirality* **17**, 421–437 (2005). URL <https://onlinelibrary.wiley.com/doi/abs/10.1002/chir.20179>.
9. Belkin, M. A., Kulakov, T. A., Ernst, K.-H., Yan, L. & Shen, Y. R. Sum-frequency vibrational spectroscopy on chiral liquids: A novel technique to probe molecular chirality. *Phys. Rev. Lett.* **85**, 4474–4477 (2000). URL <https://link.aps.org/doi/10.1103/PhysRevLett.85.4474>.
10. Belkin, M. A., Han, S. H., Wei, X. & Shen, Y. R. Sum-frequency generation in chiral liquids near electronic resonance. *Phys. Rev. Lett.* **87**, 113001 (2001). URL <https://link.aps.org/doi/10.1103/PhysRevLett.87.113001>.
11. Lux, C. *et al.* Circular dichroism in the photoelectron angular distributions of camphor and fenchone from multiphoton ionization with femtosecond laser pulses. *Angewandte Chemie International Edition* **51**, 5001–5005 (2012). URL <http://dx.doi.org/10.1002/anie.201109035>.
12. Patterson, D., Schnell, M. & Doyle, J. M. Enantiomer-specific detection of chiral molecules via microwave spectroscopy. *Nature* **497**, 475–477 (2013). URL <http://dx.doi.org/10.1038/nature12150>. Letter.
13. Janssen, M. H. M. & Powis, I. Detecting chirality in molecules by imaging photoelectron circular dichroism. *Phys. Chem. Chem. Phys.* **16**, 856–871 (2014). URL <http://dx.doi.org/10.1039/C3CP53741B>.

14. Lux, C., Wollenhaupt, M., Sarpe, C. & Baumert, T. Photoelectron circular dichroism of bicyclic ketones from multiphoton ionization with femtosecond laser pulses. *ChemPhysChem* **16**, 115–137 (2015). URL <http://dx.doi.org/10.1002/cphc.201402643>.
15. Comby, A. *et al.* Relaxation dynamics in photoexcited chiral molecules studied by time-resolved photoelectron circular dichroism: Toward chiral femtochemistry. *The Journal of Physical Chemistry Letters* **7**, 4514–4519 (2016). URL <https://doi.org/10.1021/acs.jpclett.6b02065>. PMID: 27786493.
16. Yachmenev, A. & Yurchenko, S. N. Detecting chirality in molecules by linearly polarized laser fields. *Physical review letters* **117**, 033001 (2016).
17. Eibenberger, S., Doyle, J. & Patterson, D. Enantiomer-specific state transfer of chiral molecules. *Phys. Rev. Lett.* **118**, 123002 (2017). URL <https://link.aps.org/doi/10.1103/PhysRevLett.118.123002>.
18. Beaulieu, S. *et al.* Photoexcitation circular dichroism in chiral molecules. *Nature Physics* (2018). URL <https://doi.org/10.1038/s41567-017-0038-z>.
19. Owens, A., Yachmenev, A., Yurchenko, S. N. & Küpper, J. Climbing the rotational ladder to chirality. *Physical review letters* **121**, 193201 (2018).
20. Yachmenev, A., Onvlee, J., Zak, E., Owens, A. & Küpper, J. Field-induced diastereomers for chiral separation. *Physical review letters* **123**, 243202 (2019).

21. Sakaki, K. *et al.* A suicide enzyme catalyzes multiple reactions for biotin biosynthesis in cyanobacteria. *Nature Chemical Biology* (2020). URL <https://doi.org/10.1038/s41589-019-0461-9>.
22. Spaldin, N. A. A beginner's guide to the modern theory of polarization. *Journal of Solid State Chemistry* **195**, 2 – 10 (2012). URL <http://www.sciencedirect.com/science/article/pii/S0022459612003234>. Polar Inorganic Materials: Design Strategies and Functional Properties.
23. Hickstein, D. D. *et al.* Non-collinear generation of angularly isolated circularly polarized high harmonics. *Nature Photonics* **9**, 743–750 (2015). URL <https://doi.org/10.1038/nphoton.2015.181>.
24. Pisanty, E. *et al.* High harmonic interferometry of the lorentz force in strong mid-infrared laser fields. *New Journal of Physics* **20**, 053036 (2018). URL <https://doi.org/10.1088/2F1367-2630%2Faabb4d>.
25. Ayuso, D. *et al.* Synthetic chiral light for efficient control of chiral light-matter interaction. *Nature Photonics* **13**, 866–871 (2019). URL <https://doi.org/10.1038/s41566-019-0531-2>.
26. Neufeld, O. *et al.* Ultrasensitive chiral spectroscopy by dynamical symmetry breaking in high harmonic generation. *Phys. Rev. X* **9**, 031002 (2019). URL <https://link.aps.org/doi/10.1103/PhysRevX.9.031002>.

27. Brixner, T. & Gerber, G. Femtosecond polarization pulse shaping. *Optics letters* **26**, 557–559 (2001).
28. Garg, M., Kim, H.-Y. & Goulielmakis, E. Ultimate waveform reproducibility of extreme-ultraviolet pulses by high-harmonic generation in quartz. *Nature Photonics* **12**, 291–296 (2018).
29. Hernández-García, C. *et al.* Extreme ultraviolet vector beams driven by infrared lasers. *Optica* **4**, 520–526 (2017).
30. Cameron, R. P., Yao, A. M. & Barnett, S. M. Diffraction gratings for chiral molecules and their applications. *The Journal of Physical Chemistry A* **118**, 3472–3478 (2014). URL <https://doi.org/10.1021/jp500319x>. PMID: 24655409.